Glioblastoma invasion relies on actomyosin contractility and metalloproteinase activity

Hyeje Sumajit[1], David Böhringer[2], Branko Stefanovic[1], Christoph Mark[2]*, Jerome Irianto[1]*

[1] Department of Biomedical Sciences, College of Medicine, Florida State University, Tallahassee, FL, USA
[2]Friedrich-Alexander University Erlangen-Nürnberg, Department of Physics, Erlangen, Germany

*co-corresponding author:
Jerome Irianto, Phone: +1-850-645-9438, Email: jerome.irianto@med.fsu.edu
Christoph Mark, Phone: +49-9131-85-25604, Email: christoph.mark@fau.de

Abstract

Glioblastoma multiforme (GBM) is one of the most aggressive and invasive types of brain tumors with a 5-year survival rate of less than 20%. Due to its highly invasive phenotype, GBM cells tend to invade the surrounding normal brain tissue, making it challenging to fully resect the tumor and resulting in a relapse of the disease even after surgery. Hence, it is crucial to improve our mechanistic understanding of GBM invasion phenotype, in the hope of inhibiting the disease progression. Here, we used patient-derived GBM neurospheres as a model to study GBM invasion. When these neurospheres were cultured in Matrigel, the GBM cells spontaneously invaded the surrounding microenvironment. We first characterized the invasion rate through live imaging and the forces exerted by cells as they invade the Matrigel using traction force microscopy (TFM) analysis. We observed a significant increase in cellular contractility as the cells invaded the surrounding Matrigel, prompting us to investigate the role of myosin in the cell invasion. To test this, the GBM neurospheres were treated with a myosin inhibitor, Blebbistatin. Myosin inhibition led to reduced GBM invasion and contractility. Furthermore, we investigated the role of metalloproteinases (MMPs) and showed that GBM invasion relies on MMP activity in the absence of myosin. Together, this data shows the interplay between myosin and MMPs in GBM invasion.

Introduction

Glioblastoma multiforme (GBM) is one of the most aggressive and invasive types of brain tumors with a 5-year survival rate of less than 20% [1]. Unlike other solid cancers, GBM rarely metastasizes outside the brain, but infiltrates into healthy brain tissue through the perivascular space and brain parenchyma [2-5]. Standard treatment of care includes complete surgical resection followed by radiation and chemotherapy with temozolomide (TMZ). However, due to its highly invasive phenotype, fully resecting the tumor is a challenge and any remaining tumor cells will give rise to a relapse of the disease. Improving our understanding of GBM invasion is critical to develop new therapeutic approaches for more effective interventions in containing this disease.

Cell migration has been heavily studied in cancer research due to the ability of these cells to metastasize and invade other distant parts of the body. In two-dimensional (2D) culture, cell migration has been characterized as a cyclic process starting from the establishment of cell polarity in the direction of movement driven by actin-based protrusions, adhesion to the extracellular matrix (ECM) via transmembrane receptors acting as traction sites for forward movement, and finishing with retraction at the rear for detachment [6, 7]. Despite what we know about the key players of cell migration in 2D substrates, 2D and three-dimensional (3D) microenvironments are vastly different depending on the physical characteristics of the ECM such as topography, ECM-ligand interactions, and elastic properties [8]. Increasing evidence shows the adaptability of cancer cells to switch to different migration modes when cultured in 3D-ECMs [9]. Others also show the differential effects of myosin-II-driven contractile forces in gliomas when cultured in 2D vs 3D matrix suggesting the complexity of the GBM microenvironment and the additional factors driving cell migration [10-12].

Here, we used patient-derived GBM neurospheres as a 3D model to study GBM invasion. We observed spontaneous protrusions and migration of cells when these neurospheres were cultured in Matrigel. To characterize the invasion rate and their behavior against its surroundings, we implemented the use of traction force microscopy (TFM) analysis and measured the contractile forces that the cells generate during cell movement. Our results showed that the contractility of GBM cells significantly relies on myosin II. However, a degree of invasion was still evident in the blebbistatin-treated cells which led us to further investigate the role of metalloproteinases (MMPs) in GBM invasion using pan-MMP inhibitor, GM 6001. Interestingly, our results showed that the persistence of GBM invasion relies on MMP activity during myosin inhibition. Together, we show the roles of myosin II and MMPs in cell contractility and GBM invasion.

Results and discussions

GBM neurospheres spontaneously invade their surrounding environment

To study GBM invasion, we used patient-derived GBM neurospheres, PDM-140, as a 3D-GBM model isolated from primary glioblastoma brain tissue obtained from the Human Cancer Models Initiatives (HCMI). These neurospheres are normally propagated in suspension with GBM culture medium and growth factors in low attachment 6-well plates. Microscopy imaging shows that when PDM-140 is cultured in Matrigel, a basement membrane matrix rich in ECM proteins, it forms elongated protrusions and pseudopodial structures at the leading edge to facilitate cell movement (**Figure 1A**). At day 0, which is the time after seeding neurospheres in Matrigel domes, GBM cluster and individual cells around the area showed a circular shape. 24h after, indicated as day 1, several cells in the periphery of the cluster started forming protrusions in the direction of movement. By day 2, we observed interconnectivity between invading cells as a result of its invasive nature.

In addition, confocal images show prominent actin-based protrusions at the periphery of the cells, as well as microtubule networks along the cell (**Figure 1B**). Cells grown in collagen-rich 3D matrix displayed similar dendritic pseudopodial protrusions as opposed to lamellipodia or filopodia formation in 2D substrates [13]. We also observed that the actin protrusion at the leading edge of the cell extends beyond the microtubule tips, but both are in close proximity to each other. Dugina et al. revealed selective interaction between microtubules and cytoplasmic actin via microtubule plus-end-tracking proteins (+TIPs) EB1 which correlated with glioblastoma progression and migratory potential [14, 15]. Microtubule function in cell motility was further elucidated in 3D cell migration studies performed in soft substrates showing reliance of pseudopod-based cell elongation on microtubules [13, 16, 17].

Next, we characterized the invasion potential of GBM neurospheres using live-cell microscopy and tracked the motility of cells. Neurospheres embedded in Matrigel were seeded on a 48-well plate and were imaged every 30 minutes for 48 hours. Significant phenotypic changes and cell movement were more pronounced between day 1 and day 2, which is why we focused on tracking the migration of cells within this interval. Using MTrackJ, a manual tracking plugin on ImageJ [18], we tracked individual invading cells within a 15-hour time period and plotted cell trajectories of measured x and y positions normalized to a single origin (**Figure 1C**). Trajectories of 30 cells showed linear and forward direction of movement with total distance plotted in a distribution curve (**Figure 1D**). The velocity of cells was measured over time and the results displayed a steady motility behavior within the recorded time-period. Overall, our 3D patient-derived GBM model showed a highly invasive phenotype when cultured in an ECM-rich matrix

characterized by pseudopod that is enriched for actin protrusion and microtubule network.

TFM analysis reveals the high contractility of GBM neurospheres

The extensive actin protrusions of the invading cells suggest the interaction between the cell and the surrounding Matrigel. To investigate the characteristics of this interaction, we performed 3D TFM analysis [19, 20] on the GBM neurospheres. TFM workflow involves the use of fiducial markers (e.g. fluorescent beads) to measure material deformation by comparing the original position of markers to the deformed state. By considering the material mechanical properties and the marker displacement as a proxy for matrix deformations, we reconstruct 3D forces exerted by the cells onto the material. We used 3D TFM to quantify the force exerted by the invading GBM cells onto the surrounding Matrigel. GBM neurospheres were stained with a live-cell actin probe, SPY-555 Actin, and embedded within Matrigel seeded with 0.2 µm fluorescence beads. Using confocal live-imaging for 48 hours at 30-minute intervals, the invasion of cells can be observed through actin imaging, while the displacement of the beads reflected matrix deformation (**Figure 2A**). The accumulation of beads around the cluster over time suggests the contraction of cells towards the cluster as the cells invade. Indeed, through the displacement vector fields, we observed extensive bead displacement as the cells invaded over time (**Figure 2B-C**). The 3D TFM analyses on three independent neurospheres revealed a gradual increase in contractility over time (**Figure 2D**). Interestingly, contractility increases more rapidly during the first 24 hours after seeding, a period when less invasion is observed. This suggests that GBM cells must first build up high contractility at the early stage of the invasion process, while the later stages of invasion require lower contractility.

Inhibition of myosin activity suppresses GBM invasion and contractility

Motor protein, myosin II, is known to mediate cell contractility in both 2D and 3D cultures through actomyosin-dependent cellular contractility. Hence, it is likely that the increase in contractility that we observed here relies on myosin contractility. To investigate the role of myosin II in GBM invasion, we treated GBM neurospheres cultured in Matrigel with 200µM Blebbistatin for 3 days. Blebbistatin is a myosin II inhibitor that selectively binds to the myosin-ADP-P_i complex slowing down the release of phosphate and preventing rigid actomyosin cross-linking [21]. Control cells were treated with the DMSO vehicle and similar to what we observed in Figure 1A, GBM neurospheres formed elongated protrusions and spontaneously invaded the Matrigel (**Figure 3A**). After the Blebbistatin treatment, the elongated cellular morphology of the

invading cells was still observed, however, we observed much less invasion when compared to the control. The difference in invasion potential between these two conditions was quantitatively reflected in cell trajectories measured by tracking invading cells over time (**Figure 3B**). The direction of cell movement is still linear, but the invasion distance is significantly suppressed compared to control. The invasion in Blebbistatin-treated cells was significantly shorter (44.16±3.36 µm vs 70.21±4.97 µm) and much slower (0.05±0.01 µm/min vs 0.08±0.01 µm/min) compared to control (**Figure 3Biii**). These results suggest the reliance of GBM neurosphere invasion on myosin activity. Seeing this phenotypic change, we asked whether cell contractility in GBM neurospheres was driven by myosin II. Performing the same TFM analysis as previously described, deformation vector images showed that Blebbistatin significantly suppresses the contractility of cells (**Figure 3C-D**). In contrast with what we observed in Figure 2B, the accumulation of beads around the cluster was less pronounced depicting the inability of cells to generate enough force that can displace the surrounding beads in the area. Altogether, we showed that GBM invasion and contractility are dependent on myosin II activity.

GBM invasion during myosin inhibition relies on metalloproteinases (MMPs) activity

To note, a degree of invasion is still observed after the myosin inhibition by Blebbistatin. Looking closer at these invading cells, we realized that the contractility around these cells is relatively very low when compared to the invading cells in the control sample (**Figure 3C, arrow**). This suggests a mode of invasion that does not rely on myosin contractility, making us wonder what mechanism enables such migration. Remodeling of ECM proteins by cancer cells is an important factor in metastasis. Cancer cells and other cells in the tumor microenvironment (such as immune cells and fibroblasts) secrete MMPs to digest the surrounding ECM proteins, which in turn facilitates cell migration and metastasis. To investigate the role of MMP in GBM neurosphere invasion, the neurospheres were treated with a universal MMP inhibitor, 20µM GM 6001, and were imaged for 3 days. Neurospheres were treated with a universal MMP inhibitor, 20µM GM 6001, and were imaged for 3 days. Brightfield images of control and GM 6001-treated cells show similar invasive phenotypes and did not show significant differences in their invasion distance and velocity (**Figure 4A-D**). Interestingly, when we treated the neurospheres with a combination of 20µM GM 6001 and 100µM Blebbistatin drug inhibitors, we observed a significant reduction in both invasion distance and velocity, even less than what we observed with Blebbistatin-treated cells alone. This suggests that the invasion observed during myosin inhibition relies on MMP activity and implies that the GBM cells can remodel the surrounding microenvironment to allow invasion with low cellular contractility. Nevertheless, the invasion was not perturbed by

MMP inhibition alone, suggesting that GBM cellular contractility can overcome the absence of MMP activity. Combined, our results show the dependence of GBM invasion on both cellular contractility and MMP activity, and the relationship between these two processes.

Conclusion

In conclusion, our 3D patient-derived GBM model exhibited a highly invasive and contractile phenotype when cultured in an ECM-rich matrix, characterized by pseudopods enriched with actin protrusions and a microtubule network. In addition, our study showed the critical roles of myosin II and MMPs in GBM contractility and invasion. We provide evidence that GBM invasion relies on MMP activity to remodel its surrounding environment and facilitate cellular motility in the absence of myosin. Collectively, our findings provide a premise for further investigations on myosin II and MMP activities as a potential target for inhibiting GBM invasion.

Materials and methods

Cell culture

Patient-derived GBM neurospheres, HCM-BROD-0195-C71 (ATCC PDM-140) were generated by the Human Cancer Models Initiative (HCMI) and acquired from ATCC. The GBM neurospheres were cultured in complete medium containing NeuroCult NS-A Basal Medium (StemCell Technologies #05750) with NS-A Proliferation Supplement (StemCell Technologies #05753), 20ng/mL EGF (Peprotech #AF-100-15), 20ng/mL bFGF (StemCell Technologies #78003.1), and 2µg/mL Heparin (StemCell Technologies #07980) on a non-adherent 6-well plate (Corning #3814). Maintenance and cryopreservation were performed following the instructions from ATCC.

For the drug inhibitors treatment, neurospheres were cultured in Matrigel on a 48-well plate. Drug inhibitors Blebbistatin (100µM, MilliporeSigma) and pan-MMP inhibitor GM 6001 (20µM, MilliporeSigma) were diluted in complete GBM medium and added to wells. Neurospheres were treated with drug inhibitors for 3 days and growth and invasion were monitored by taking daily images with z-stacking using Olympus IX71, 10X/0.3NA. All image analysis were performed using ImageJ [18].

Live-cell imaging and cell tracking

GBM neurospheres were cultured in Matrigel and seeded on a 48-well plate with the different conditions (drug inhibitors used). Using Olympus IX71 and 10X/0.3NA objective, live-imaging was setup for 15 hours at 30min-intervals. During image processing, 5 ROIs (region of interest) were selected for each condition for the cell tracking analysis. MTrackJ was used to manually track movement of cells from each timepoint for a total of 15 hours [22]. Cell trajectories were plotted on Graphpad Prism 10 using the x and y measured values from ImageJ.

Traction force microscopy (TFM) analysis

For the experimental set-up, GBM neurospheres were seeded at 15,000 cells per 15µL Matrigel domes on an 8-well Lab-Tek glass chambered coverglass (Thermo Scientific #155409PK). Matrigel and 0.2µm carboxylate fluorescent beads (Thermo Scientific #F8810) solution in a 1:600 dilution was prepared first before addition of cells to form respective domes. To track migration of cells, neurospheres were stained with SPY-actin (1:4000 dilution in complete GBM media) and added to wells. All live cell imaging were performed using Andor Revolution Spinning Disk Laser Confocal Microscope with a 20X/0.75NA objective.

Neurosphere traction forces are reconstructed from time-lapse image stacks using the open-source program Saenopy [19]. Image stacks of fluorescent beads embedded in matrigel with a voxel size of 0.69µm x 0.69µm x 2.0µm and a time delta of 30min between consecutive recordings are loaded in the analysis pipeline of Saenopy, and deformations between consecutive stacks are determined by particle image velocimetry using a window size of 20 pixels (the element size is set to 15 pixels, the signal-to-noise threshold to 1.3, and drift correction is applied). The resulting 3D deformations fields between consecutive stacks are then accumulated to obtain the total deformation field at each point in time. These accumulated deformation fields are then interpolated to a regular grid with a spacing of 7µm and a size of 300µm x 300µm x 150µm for further processing. The interpolated deformations fields are used by the iterative force reconstruction algorithm to derive the 3D force fields that best describe the observed deformations at each point in time. The material parameters for Matrigel are obtained by rotational rheology as k_0=675 Pa (linear stiffness), d_0=1.0 (buckling coefficient), d_s=0.275 (strain stiffening coefficient), and λ_s=0.175 (strain stiffening onset). From the reconstructed 3D force fields, we compute the neurosphere contractility by projecting the individual force vectors towards the epicenter of the deformation fields and summing up the projected force vectors.

Immunofluorescence staining

Hydrogels were fixed in 2% paraformaldehyde (VWR) and 1% glutaraldehyde (VWR) for 20 min, permeabilized in 0.5% Triton X-100 (MilliporeSigma) for 10 min and blocked with 5% bovine serum albumin (VWR) for 30 min. Samples were incubated with primary antibody targeting α-tubulin (SigmaAldrich # T9026, DM1A mouse monoclonal) overnight at 4°C and secondary antibody for 2 hours at RT. Cells were incubated with 2µg/mL DAPI and phalloidin-tetramethylrhodamine B isothiocyanate (Sigma-Aldrich) for 1 hour to stain for nuclei and F-actin. Images were taken using Zeiss LSM 880 Confocal Microscope (Plan-Apochromat 63x/1.40 Oil DIC M27).

Statistical analysis

All graphs and analyses were generated using Graphpad Prism 10. Figure legends specify the sample size for each condition. Statistical analyses were conducted using paired t-test and one-way analysis of variance (ANOVA) with Tukey multiple comparison test. All statistical tests were considered significant if $p < 0.05$. All plots show Mean±SEM.

Acknowledgements

The authors would like to thank the Confocal Microscopy Laboratory at FSU College of Medicine for access to the confocal microscopes. The authors would like to thank Dr. Terra Bradley for the careful editing of the manuscript. The authors would like to thank all lab members in Dr. Jerome Irianto's and Dr. Yue Julia Wang's lab for their support and valuable suggestions in reviewing the manuscript. HS, JI, and BS were supported by startup funds from Florida State University, an award from the Institute of Pediatric Rare Diseases (FSU College of Medicine), and awards from the Florida Department of Health's Bankhead-Coley Cancer Research Program (award number 21B11), and Live Like Bella Pediatric Cancer Research Initiative (award number 23L06). The GBM neurospheres are from the Human Cancer Models Initiative (HCMI), https://ocg.cancer.gov/programs/HCMI.

REFERENCES

1. Das, K.K. and R. Kumar, *Pediatric Glioblastoma*. Glioblastoma, ed. S.D. Vleeschouwer. 2017, Brisbane (AU).

2. Vishnu Anand Cuddapah, S.R., Stacey Watkins & Harald Sontheimer *A neurocentric perspective on glioma invasion*. Nature Reviews Neuroscience, 2014. **15**: p. 455-465.

3. Faisal, S.M., et al., *Spatiotemporal Insights into Glioma Oncostream Dynamics: Unraveling Formation, Stability, and Disassembly Pathways*. Advanced Science, 2024. **11**(18): p. 2309796.

4. Pavlo G. Gritsenko, O.I., Peter Friedl, *Interstitial guidance of cancer invasion*. The Journal of Pathology, 2012.

5. Osswald, M., et al., *Brain tumour cells interconnect to a functional and resistant network*. Nature, 2015. **528,7580** p. 93-98.

6. Caswell, P.T. and T. Zech, *Actin-Based Cell Protrusion in a 3D Matrix*. Trends in Cell Biology, 2018. **Volume 28**(Issue 10): p. 823 - 834.

7. Anne J. Ridley, M.A.S., Keith Burridge, Richard A. Firtel, Mark H. Ginsberg, Gary Borisy, J. Thomas Parsons, and Alan Rick Horwitz, *Cell Migration: Integrating Signals from Front to Back*. Science, 2003. **302**(5651): p. 1704-1709.

8. Doyle, A.D., et al., *Dimensions in Cell Migration*. Current opinion in cell biology 2013. **Current opinion in cell biology vol. 25,5** p. 642-649. .

9. Friedl, P. and S. Alexander, *Cancer Invasion and the Microenvironment: Plasticity and Reciprocity.* Cell, 2011. **Volume 147**(Issue 5): p. 992 - 1009.

10. Gabrielle Faure-André, P.V., Maria-Isabel Yuseff, Mélina Heuzé, Jheimmy Diaz, Danielle Lankar, Veronica Steri, Jeremy Manry, Stéphanie Hugues, Fulvia Vascotto, Jérôme Boulanger, Graça Raposo, Maria-Rosa Bono, Mario Rosemblatt, Matthieu Piel , and Ana-Maria Lennon-Duménil, *Regulation of Dendritic Cell Migration by CD74, the MHC Class II-Associated Invariant Chain*. Science, 2008. **322**(5908): p. 1705-1710.

11. Wylie, S.R. and P.D. Chantler, *Myosin IIC: A Third Molecular Motor Driving Neuronal Dynamics*. Molecular Biology of the Cell, 2008. **19**(9).

12. Christopher Beadle, M.C.A., Pascale Monzo, Richard Vallee, Steven S. Rosenfeld, and Peter Canoll, *The Role of Myosin II in Glioma Invasion of the Brain*. Molecular Biology of the Cell, 2008. **19**(8).

13. Giri, A., et al., *The Arp2/3 complex mediates multigeneration dendritic protrusions for efficient 3-dimensional cancer cell migration*. FASEB journal : official publication of the Federation of American Societies for Experimental Biology, 2013. **27(10)**: p. 4089–4099.

14. Berges, R., et al., *End-binding 1 protein overexpression correlates with glioblastoma progression and sensitizes to Vinca-alkaloids in vitro and in vivo.* Oncotarget, 2014. **vol. 5,24**: p. 12769-87.

15. Dugina, V., et al., *Interaction of microtubules with the actin cytoskeleton via cross-talk of EB1-containing +TIPs and γ-actin in epithelial cells*. Oncotarget, 2016. **vol. 7,45** p. 72699-72715.

16. Bouchet, B.P., et al., *Mesenchymal Cell Invasion Requires Cooperative Regulation of Persistent Microtubule Growth by SLAIN2 and CLASP1*. Developmental Cell, 2016. **39**: p. 708-723.

17. Peter Friedl, E.S., Stephen Weiss & Kenneth M. Yamada *New dimensions in cell migration*. Nature Reviews Molecular Cell Biology, 2012. **13**: p. 743-747.

18. Johannes Schindelin, I.A.-C., Erwin Frise, Verena Kaynig, Mark Longair, Tobias Pietzsch, Stephan Preibisch, Curtis Rueden, Stephan Saalfeld, Benjamin Schmid, Jean-Yves Tinevez, Daniel James White, Volker Hartenstein, Kevin Eliceiri, Pavel Tomancak & Albert Cardona, *Fiji: an open-source platform for biological-image analysis*. Nature Methods, 2012. **9**: p. 676-682.

19. David Böhringer, M.C., Lars Bischof, Tina Czerwinski, Niklas Gampl, Phuong Anh Ngo, Andreas Bauer, Caroline Voskens, Rocío López-Posadas, Kristian Franze, Silvia Budday, Christoph Mark, Ben Fabry & Richard Gerum, *Dynamic traction force measurements of migrating immune cells in 3D biopolymer matrices*. Nature Physics, 2024.

20. Mark, C., et al., *Collective forces of tumor spheroids in three-dimensional biopolymer networks*. Elife, 2020.

21. Kovács, M.l., et al., *Mechanism of Blebbistatin Inhibition of Myosin II*. Journal of Biological Chemistry, 2004. **Volume 279**(Issue 34): p. 35557 - 35563.

22. E. Meijering, O.D., I. Smal, *Methods for Cell and Particle Tracking*. Methods in Enzymology, 2012. **504**.

Figure 1

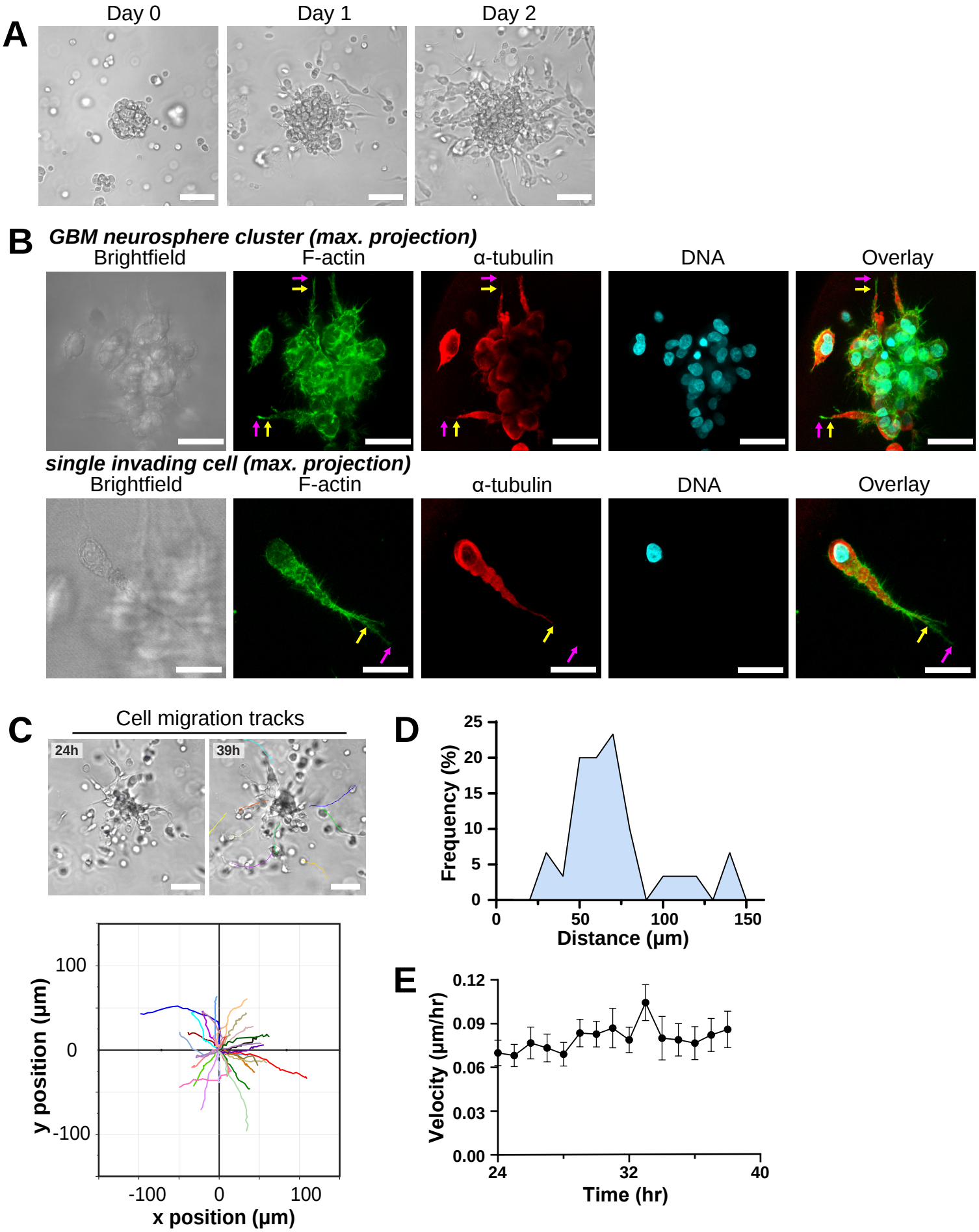
A
Day 0
Day 1
Day 2
B
GBM neurosphere cluster (max. projection)
Brightfield
F-actin
α-tubulin
DNA
Overlay
single invading cell (max. projection)
Brightfield
F-actin
α-tubulin
DNA
Overlay
C
Cell migration tracks
24h
39h
100
0
-100
y position (μm)
-100
0
100
x position (μm)
D
25
20
15
10
5
0
Frequency (%)
0
50
100
150
Distance (μm)
E
0.12
0.09
0.06
0.03
0.00
Velocity (μm/hr)
24
32
40
Time (hr)

Figure 1. Invasive phenotype of patient-derived GBM neurospheres

(A) Brightfield images of GBM neurospheres cultured in Matrigel for 3 days showing cell invasiveness as it forms elongated protrusions and pseudopodial structures to facilitate movement against its surroundings starting from day 1. Scale bar = 100µm.

(B) Maximum projection of confocal sections of GBM neurosphere cluster (top) and single invading cell (bottom) stained for F-actin (green), α-tubulin (red), and DNA (cyan) revealing prominent actin-based protrusions at the leading edge and cell-cell boundaries, and microtubule networks extending from the nucleus to the leading edge of the invading cells. Arrows showing the end location of actin (magenta) and tubulin (yellow). Scale bar = 20µm.

(C) (Top) Representative images from live imaging of invading GBM cells, which were tracked from day 1 to day 2 for a total of 15 h. Each color corresponds to an individual cell. (Bottom) Cell trajectories plotted using measured x and y positions normalized to a single origin showing spontaneous displacements of individual cells. Scale bar = 150µm; n=30 cells.

(D) Quantification of total distance traveled plotted as a frequency distribution.

(E) The averaged velocity of the invading cells over time (Mean±SEM).

Figure 2

A ***max. projection***

Time-point

0 h | 12 h | 26 h | 33 h | 48 h

Cells

Beads

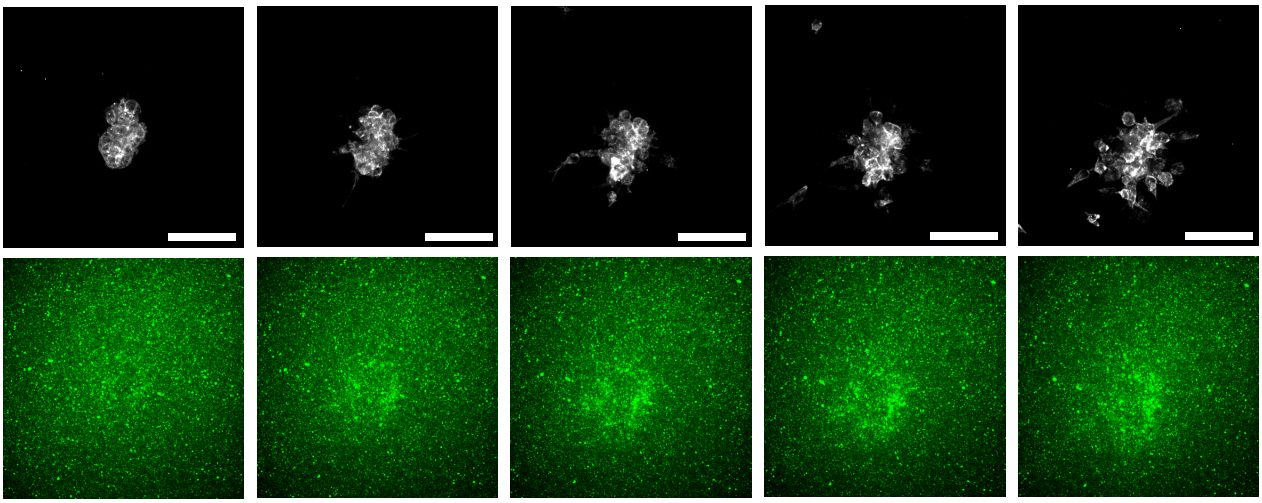

B ***single z-plane images***

Cells

Beads

2D Vector field

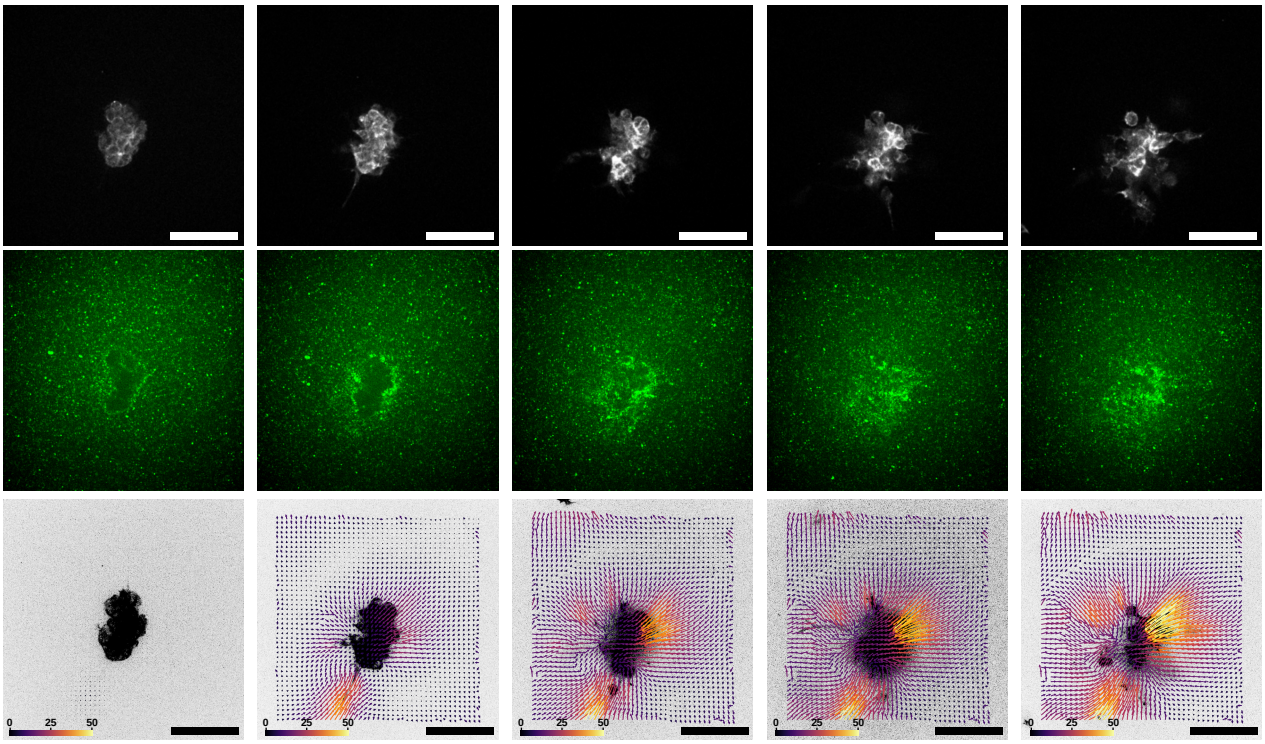

C ***3D deformation field***

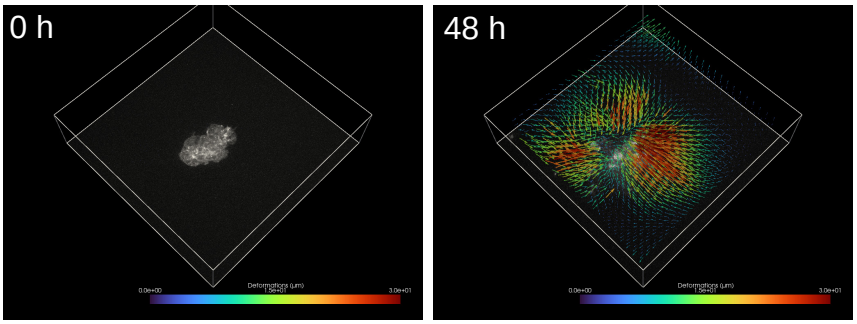

D

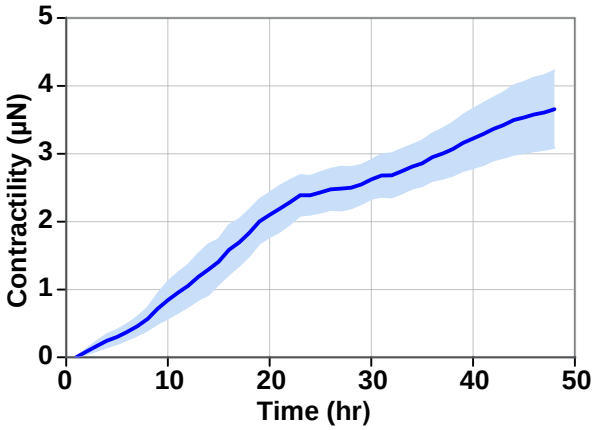

Figure 2. Traction force microscopy (TFM) analysis reveals the high contractility of GBM neurospheres.

(A) Representative maximum projections from the live confocal imaging of GBM neurospheres stained with a live-cell actin probe, SPY-555 Actin, and embedded within Matrigel seeded with 0.2 µm fluorescence beads. The invasion of the cells can be observed through actin imaging, while the displacement of the beads indicates the cell-to-matrigel interactions. The accumulation of beads around the cluster over time suggests the contraction of cells towards the cluster as the cells invade. Scale bar = 100 µm.

(B) Images of corresponding GBM neurosphere, fluorescent beads, and 2D displacement vector field at a single z-plane in different timepoints. In the 2D deformation field images, arrows indicate the direction of the matrix deformations and changes in color indicate the magnitude of deformations (0 to 50µm). Scale bar = 100 µm.

(C) 3D deformation field of the corresponding GBM neurosphere embedded at 0h or 48h measurement time. Arrows indicate the direction of the matrix deformations; the color of the arrows indicates the magnitude of the matrix deformations (0 to 30µm).

(D) Neurosphere contractility as a function of time, determined by 3D TFM showing an increase in contractility over time (n = 3 neurospheres, Mean ± SEM).

Figure 3

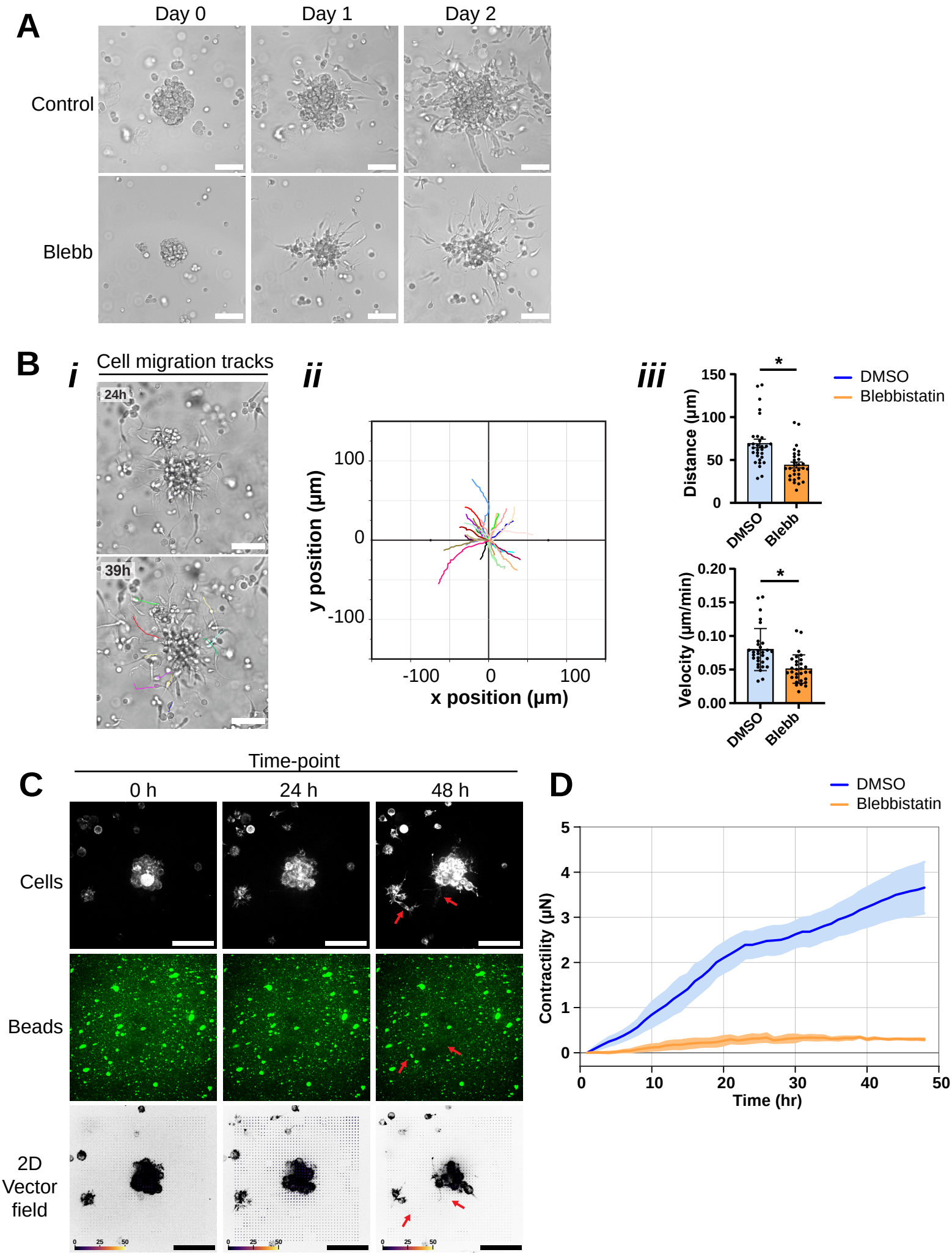
A
Day 0
Day 1
Day 2
Control
Blebb
B
i
Cell migration tracks
24h
39h
ii
y position (µm)
x position (µm)
100
0
-100
iii
Distance (µm)
150
100
50
0
DMSO
Blebb
*
Velocity (µm/min)
0.20
0.15
0.10
0.05
0.00
DMSO
Blebbistatin
C
Time-point
0 h
24 h
48 h
Cells
Beads
2D Vector field
D
DMSO
Blebbistatin
Contractility (µN)
Time (hr)
0
10
20
30
40
50
1
2
3
4
5

Figure 3. Inhibition of myosin activity suppresses GBM invasion and contractility.

(A) Brightfield images of GBM neurospheres treated with DMSO (control, top) and myosin II inhibitor, 100µM Blebbistatin, (Blebb, bottom) for 3 days. Blebbistatin-treated samples show long protrusions at the leading edge, but less invasion of cells compared to the control suggesting the dependence of GBM invasion on myosin activity. Scale bar = 100µm.

(B) (i) Representative images from live imaging of invading GBM cells, which were tracked from day 1 to day 2 for a total of 15 h. Each color corresponds to an individual cell. Scale bar = 150µm. **(ii)** Cell trajectories plotted using measured x and y positions normalized to a single origin. (n = 30 cells) **(iii)** Invasion distance (top) and velocity (bottom) of invading cells treated with DMSO (control, blue) or Blebbistatin (orange) in a 15-hour time point. Significantly lower speed and distance traveled by Blebbistatin-treated cells suggest the role of myosin II in contractility and cell movement (*$p < 0.001$, Mean±SEM).

(C) Maximum projections of GBM neurosphere and fluorescent beads, and the corresponding displacement vector field at 0h, 24h and 48h. In the 2D deformation field images, arrows indicate the direction of the matrix deformations and changes in color indicate the magnitude of deformations. Scale bar = 100 µm

(D) Comparison of contractility as a function of time between control and Blebbistatin-treated neurospheres, determined by 3D TFM showing a significantly reduced contractility over time on myosin-inhibited cells. (n = 3 neurospheres per group, Mean±SEM).

Figure 4

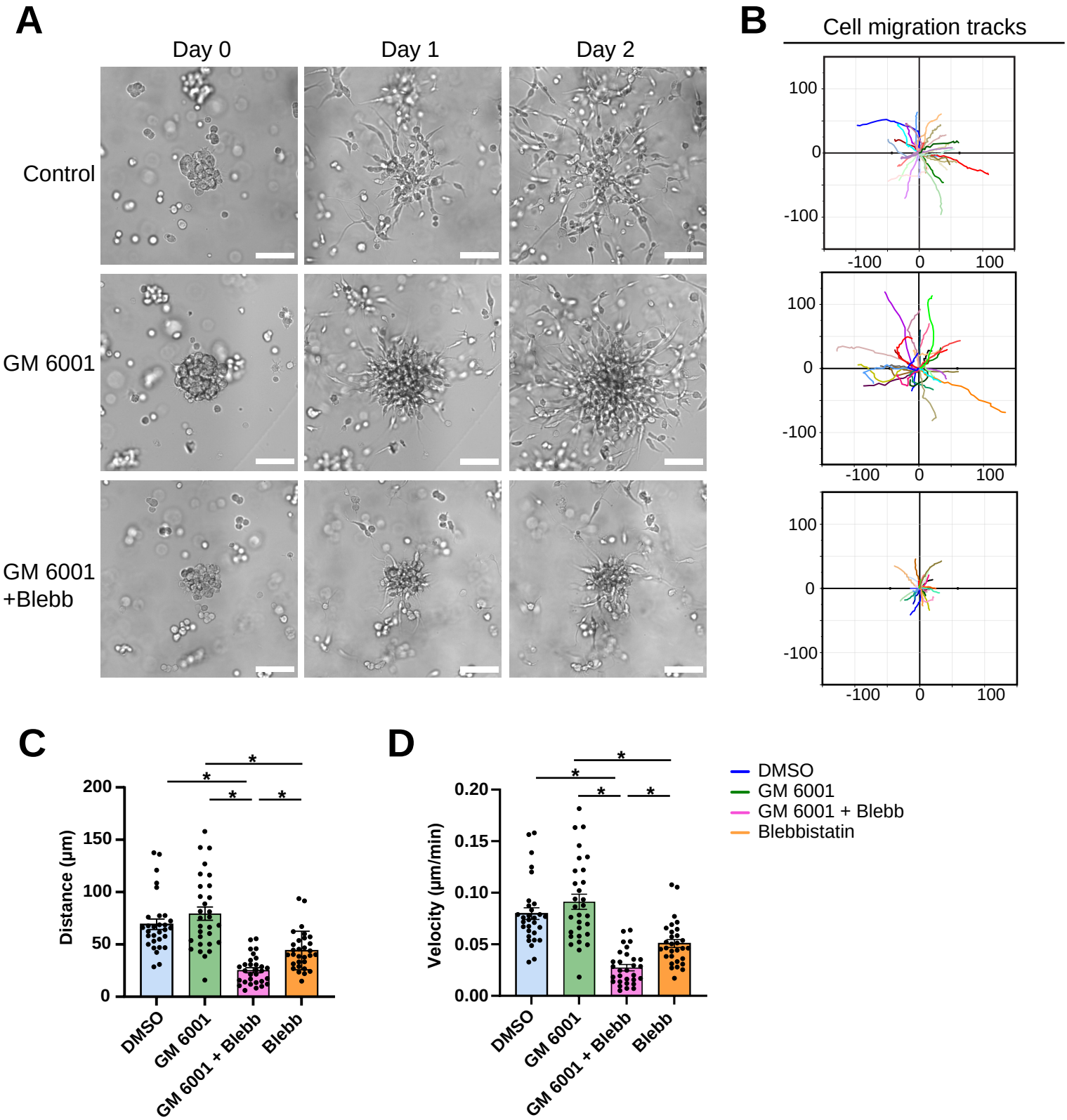
A
Day 0
Day 1
Day 2
Control
GM 6001
GM 6001
+Blebb
B
Cell migration tracks
100
0
-100
-100
0
100
C
Distance (µm)
200
150
100
50
0
DMSO
GM 6001
GM 6001 + Blebb
Blebb
D
Velocity (µm/min)
0.20
0.15
0.10
0.05
0.00
DMSO
GM 6001
GM 6001 + Blebb
Blebb
DMSO
GM 6001
GM 6001 + Blebb
Blebbistatin

Figure 4. GBM invasion during myosin inhibition relies on metalloproteinases (MMPs) activity.

(A) Brightfield images of GBM neurospheres treated with DMSO (control, top), pan-MMP inhibitor, 20µM GM 6001 (middle), and combination of 20µM GM 6001 and 100µM Blebbistatin (bottom) for 3 days. Combinatory treatment of GM 6001 and Blebbistatin showed significantly reduced GBM invasion compared to GM 6001 alone and control. No difference in invasive phenotype and cell migration was observed between GM 6001-treated cells and control. Scale bar = 100µm.

(B) Cell trajectories plotted using measured x and y positions normalized to a single origin in the different conditions mentioned in panel A. Each color corresponds to an individual cell. n=30 cells.

(C) Quantification comparing the distance traveled by migrated cells in 4 different conditions, plotted in a bar graph showing the significantly lower invasion distance in the GM 6001 + Blebbistain treated neurospheres (*$p < 0.001$, Mean±SEM). Conditions: DMSO = blue; GM 6001 = green; GM 6001 + Blebb = pink; Blebb = orange.

(D) Bar graph representation of velocity comparing 4 different conditions (DMSO = blue; GM 6001 = green; GM 6001 + Blebb = pink; Blebb = orange) *$p < 0.001$, Mean±SEM.